ASTA/NML Transverse Profile Station: Testing and Installation

A. S. Johnson, A. H. Lumpkin and R. Thurman-Keup

December 13, 2011

Abstract

A prototype transverse beam profile monitor for the superconducting rf electron linac at ASTA/NML has been successfully installed and tested at the A0 Photoinjector. The initial tests were performed at a beam energy of 15 MeV and with micropulse charges ranging from 20-500 pC. For operation at ASTA/NML, a low-power, tune-up beam will be selected from the possible 3.2 nC/bunch at 3 MHz for 1 ms at a 5 Hz repetition rate. The 4-position actuator is equipped with two intercepting radiation converter screens: a 1 μm thin Al foil for optical transition radiation and a 100 μm thick single-crystal scintillators of either YAG:Ce or LYSO:Ce. The optical system provides better than 20 μm resolution with an 18 mm vertical field of view. Installation aspects at ASTA/NML will also be addressed.

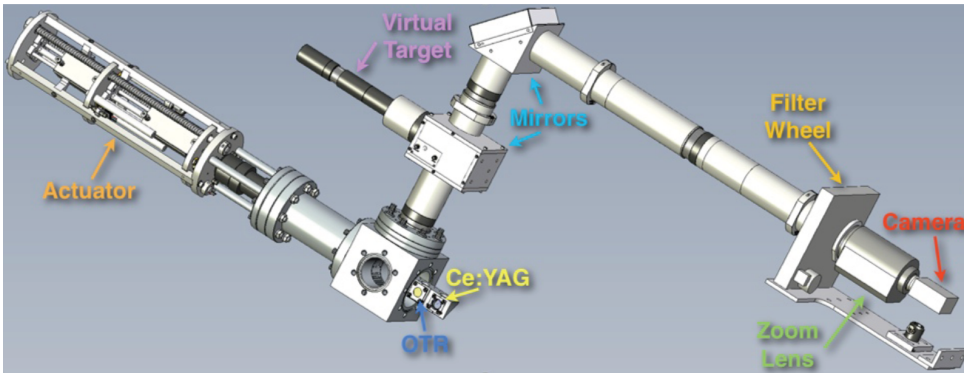

1 Introduction: ASTA/NML

Transverse beam profile monitors are being prototyped for use at a state-of-the-art complex for testing superconducting rf (SRF) cryomodules for the next generation of high intensity linear accelerators, such as the International Linear Collider (ILC) and Project-X [1]. The injection section of the accelerator consists of an L-band electron gun followed by two capture cavities, each consisting of a high-gradient, 1.3 GHz, 9-cell SRF cavity to bring the beam up to the injection energy of 40 MeV. The remainder of the beamline consists of magnets and diagnostics necessary to provide the proper beam parameters for injection into the SRF cryomodules, as shown in Figure 1. The SRF accelerator section will consist of three cryomodules each containing eight 1.3 GHz 9-cell SRF cavities, yielding a final beam energy of 810 MeV.

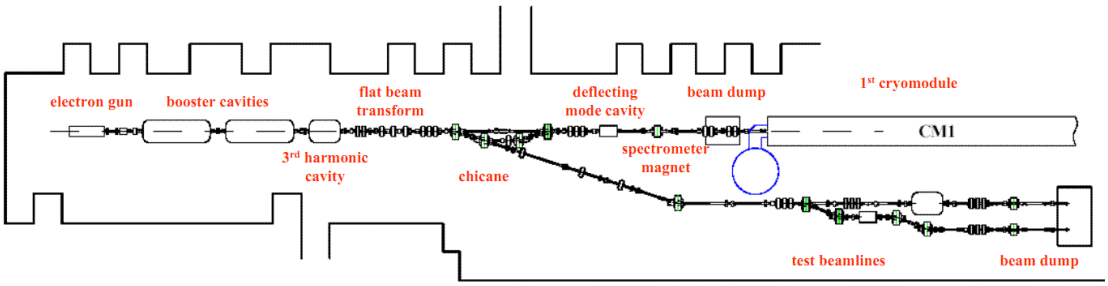

Figure 1: Injector and low energy beamline consists of 1.5 cell 1.3 GHz gun, followed by 2 9-cell scrf booster cavities, 3.9 GHz cavity, 3 skew quadrupoles for flat beam transformation, chicane, 3.9 GHz fast deflector and test beamlines.

2 Transverse Profile Monitor

A transverse beam profiling station for the characterization of low-power, tune-up beam has been initially tested at the A0 Photoinjector (A0PI) [2]. The A0PI consists of an L-band rf gun followed by a 9-cell superconducting rf capture cavity which combine to produce a 15 MeV electron beam. The charge per micropulse typically ranged from 20-500 pC and generated beam sigma sizes of 45-250 μm. The prototype station was installed in the user section of the straight ahead beamline, as shown in Figure 2.

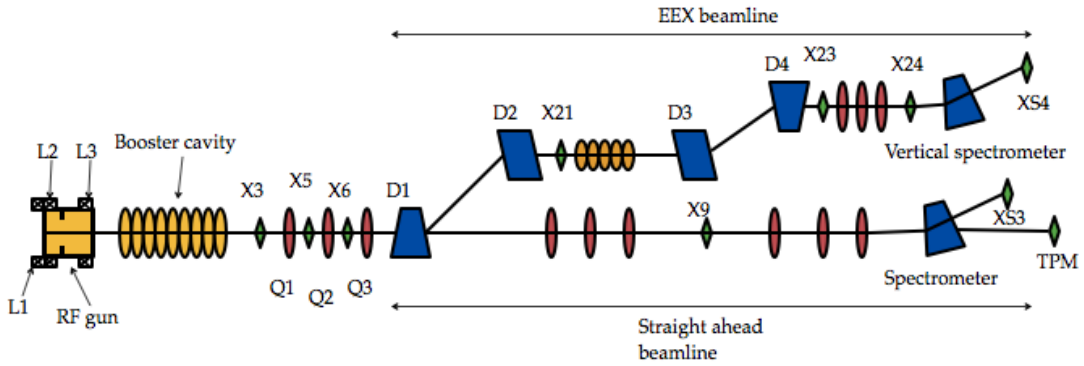

Figure 2: Schematic of the A0 Photoinjector. Elements labeled "X" are diagnostics stations (beam viewers and/or multi-slit mask locations),"L" are solenoid lenses,"Q" are quadrupole magnets ,"D" are dipole magnets and the prototype station is indicated by "TPM".

When operating with low-power, tune-up beam, intercepting radiation converter screens will be used to characterize the beam. Either a a 1 μm thin Al foil for optical transition radiation (OTR) or a 100 μm thick single-crystal scintillators of either YAG:Ce or LYSO:Ce will be inserted into the beamline. In order to reduce corrections from powder screen resolution and depth-of-focus effects previously determined at the A0PI [3], single crystal and OTR converter screens are oriented normal to the beam direction and followed by a 45° mirror to direct the radiation into the optical transport system. While reducing the scintillator screen resolution term to less than 10 μm rms and basically eliminating the depth-of-focus issue, this configuration does introduce a double source from the OTR imaging (the forward OTR from the foil and the backward OTR from the mirror). The intensity of the contributions from both sources are about equal, but the mirror source is out of focus thus adding to the measured beam size. Results from previous tests show the second image to be about 3 times larger than the focused image at this low gamma when treated with a two-Gaussian fitting procedure [2]. A method to change the optical focus to the single OTR screen in the mirror plane is being developed.

Table 1: Relevant camera parameters

CCD Imager	2/3" 5M pixels
Pixel size (μm)	3.45 × 3.45
Data Output	Gigabit Ethernet
Lens Mount	C-mount

2.1 Camera

The optical transport system is mounted on a rigid backbone and attached to the vacuum assembly, as shown in Figure 3. Radiation is transported through light-tight tubes to a 5 MegaPixel Gevicam GD-155000 CCD camera [4]. Relevant camera parameters can be found in Table 1. The prototype system installed at the A0PI used a back-illuminated virtual target with matched field lens that can be selected by inserting a beam splitter in the relay optics path. The current design will place the target pattern in the fourth position of the actuator, ensuring accurate calibration factors.

Optical resolution tests were conducted using the 5 MegaPixel camera and Fujinon 50 mm lens model HF50SA. The calibration factor of 8.8 μm/pixel was determined from a virtual target image. The virtual target was removed and a 50-μm-diameter pinhole was installed in the virtual target position to be replaced by the 25-μm and then the 15-μm diameter pinholes. The rms sizes of the apertures were estimated as diameter/$\sqrt{12}$ or 14.4 μm, 7.2 μm and 4.3 μm, respectively. The observed image sizes of 23.7 μm, 21.7 μm and 19.4 μm are consistent with sigma resolutions of 19-20 μm after subtracting the aperture sizes in quadrature. Resolution was also calculated using the USAF1951 target pattern. The modulation transfer function (MTF) was calculated for the 16 lp/mm case, by convolving a Gaussian function with an ideal square line profile to determine the sigma resolution of 20 μm.

Figure 3: Optical transport system attached to rigid backbone.

2.2 Radiation Converter Screens

Each station is equipped with both an optical transition foil and single crystal of either YAG:Ce (Ce^{3+} doped $Y_3Al_5O_{12}$) or LYSO:Ce (Ce^{3+} doped $(Lu,Y)_2SiO_5$) Table 2 lists relevant scintillator properties. Use of the intercepting screens demands beam be operated in a low-power, tune-up mode to prevent damage due to heating. In addition, the OTR foil allows beam sizes to be measured in the crystal saturation range of 0.01 pC/μm^2 [5]. Due to beam conditions at the A0PI we were unable to test the saturation limits of the crystals, but the test is planned for ASTA/NML. Experimental results comparing YAG:Ce and LYSO:Ce performances at low charge are presented in Table 3. From the table, we can see that YAG:Ce and LYSO:Ce crystals both give similar sizes of 46 μm and 54 μm, respectively, all the while maintaining equivalent intensities as indicated by the amplitudes determined by a Gaussian fit to the projected profiles.

Table 2: Comparison of scintillators for use in the TPM [5, 6, 7].

Scintillator Properties	YAG:Ce	LYSO:Ce
Index of Refraction	1.82	1.82
Wavelength of Peak Emission (nm)	525	420
Density (g/cm^3)	4.57	7.1
Photon Yield (photons/MeV)	18×10^3	25×10^3
Scintillation Efficiency (Compared to NaI)	45%	73%
Effective Atomic #	35	66

Table 3: Low charge data from both crystals. The YAG:Ce data were taken using 1 bunch with the YLF laser while the LYSO:Ce data were taken using 1 bunch generated using the UV component of the Ti:Sapph as the drive laser.

	YAG:Ce		LYSO:Ce	
	Size(μm)	Amp.	Size(μm)	Amp.
100 pC	131 ± 1.1	98.6 ± 1.4	83 ± 1.3	112 ± 1.1
20 pC	46 ± 1.2	41.4 ± 1.1	54 ± 0.1	48.6 ± 0.5

2.3 Issues

2.3.1 Heating & Saturation

Use of the single-crystal screens requires beam be operated in the low-power, tune-up mode to prevent damage due to beam heating. From the results of a simulation by Alex Murokh of RadiaBeam, for beam of 4000 pulses with charge 5 nC repeated every 1 Hz the estimated stress fracture limit of 30-40 MPa in YAG:Ce will not be reached at 20 MeV, as shown in Figure 4[8]. Of course, as noted in the conclusion of Murokh's talk, to avoid the fracture limit it is best to use less than 100, 5 nC pulses which is already enough light to saturate the CCD 1000 times over. We expect the ILC-like 3.2 nC per micropulse charge with a focus of σ<100 μm will result in scintillator saturation. This situation is expected during a quadrupole scan for emittance measturements at 250 MeV[9]. Although incoherent OTR yields only 1 photon/100 incident electrons, it is linear in response, making it suitable for beam sizes to be measured in the high-charge areal density crystal saturation range[10]. Due to beam conditions at the A0PI we were unable to test the saturation limits of the crystals, but the test is planned for ASTA/NML.

2.3.2 Microbunching

In anticipation of coherent optical transition radiation (COTR) due to the microbunching instability in the compressed beam locations at ASTA/NML, LYSO:Ce will replace YAG:Ce crystals and two filter wheels will be outfitted with bandpass and neutral density filters. Previous studies show the spectrum of COTR to be enhanced more in the red end of the spectrum [11]. In anticipation of this, we have selected LYSO:Ce crystals, which have peaked emission around 420 nm, for diagnostic stations following the chicane. Figure 5 shows the result of our bandpass filter tests. We made a horizontal stripe of 150 pC beam and recorded images with a 400×40 nm bandpass filter as shown in Figure 5a. Figure 5b shows the data in blue with a Gaussian fit in red. For the following figures 5c and 5d, we replaced the violet filter with a bandpass filter of 550×40 nm and observed a much reduced intensity, as expected. By selectively imaging at the 400 nm regime, we will mitigate contributions from the COTR.

The final test we conducted was a trigger test of the camera to show that we could image beam with the scintillators after the instantaneous peak of OTR had been emitted. Through ACNET we are able to control the

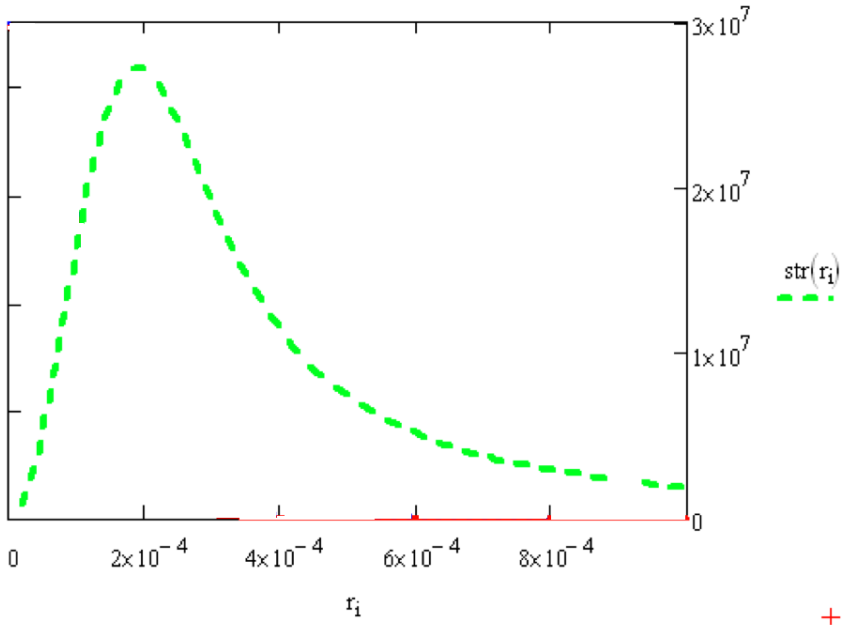

Figure 4: Plot of stress (Pascals) (right axis) versus radius for a 100 μm thick YAG screen. Simulation results of 4000 pulses of 5 nC beam with average spot size of 100 μm RMS at energy of 20 MeV.

camera trigger with parameter E:UXRTRD in order to delay from the initial value of 748.8 μs, see Figure 6a and 6d, showing LYSO:Ce and OTR images, respectively. Unfortunately the IRM does not allow for less than 100 ns changes so we added a cable delay of 41 ns as shown in Figures 6b and 6e. In these images we can see the LYSO:Ce is still visible while the OTR signal has decayed completely away. In the final set of images we have set the E:UXRTRD to 742.9 μs to show the slower decay rate of the crystal still yields a visible image, see Figures 6c and 6f. This method will work for a single micropulse at 5 Hz. If the use of bandpass filters and LYSO:Ce are not enough to reduce the COTR due to the microbunching instability, we could purchase a gated, intensified camera to observe bunch size cleanly in a pulse train by gating in burst mode at a >200 kHz rate.

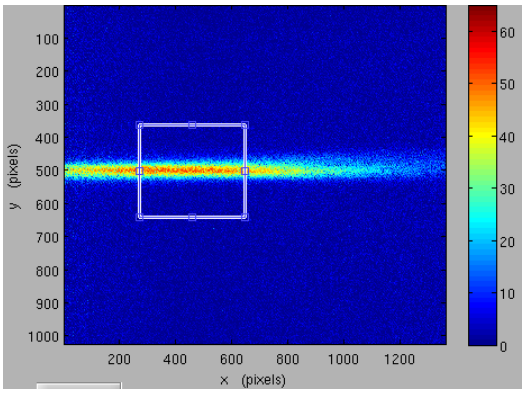

(a) Violet (400×40nm) bandpass filter

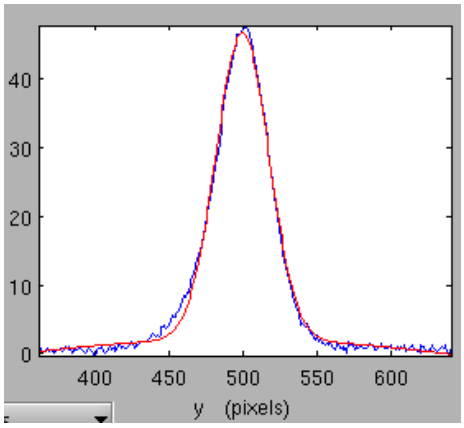

(b) Gaussian fit to the data

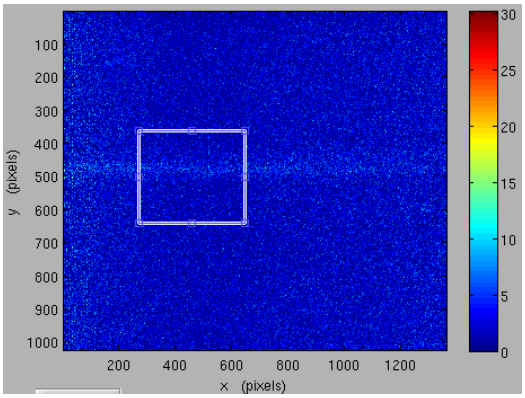

(c) Green (550×40nm) bandpass filter

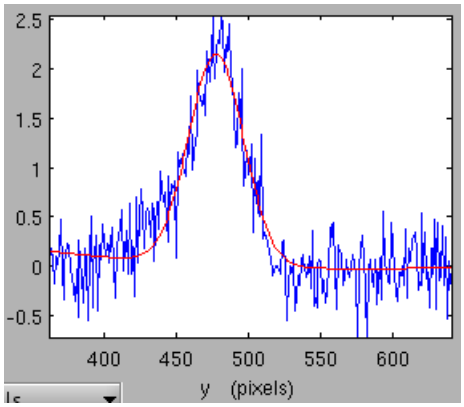

(d) Gaussian fit to tbe data

Figure 5: Filter data showing superior transmission of LYSO:Ce scintillating in the desired 400nm range.

2.3.3 OTR Point Spread Function and Polarization Effects

Another investigation started at the A0PI is that of polarization effects in beam-profiling. OTR is known to be radially polarized. Results of studies using the horizontal and vertical linear polarizers located in the filter wheel indicate that beam size may be over estimated by as much as 15% when using the total OTR signal[12]. The linear polarizer will be implemented at all stations with OTR screens. We were not able to reporduce the observed effect by modeling only the OTR point spread function for our optical set-up so we will continue with experiments at ASTA/NML. The data are consistent

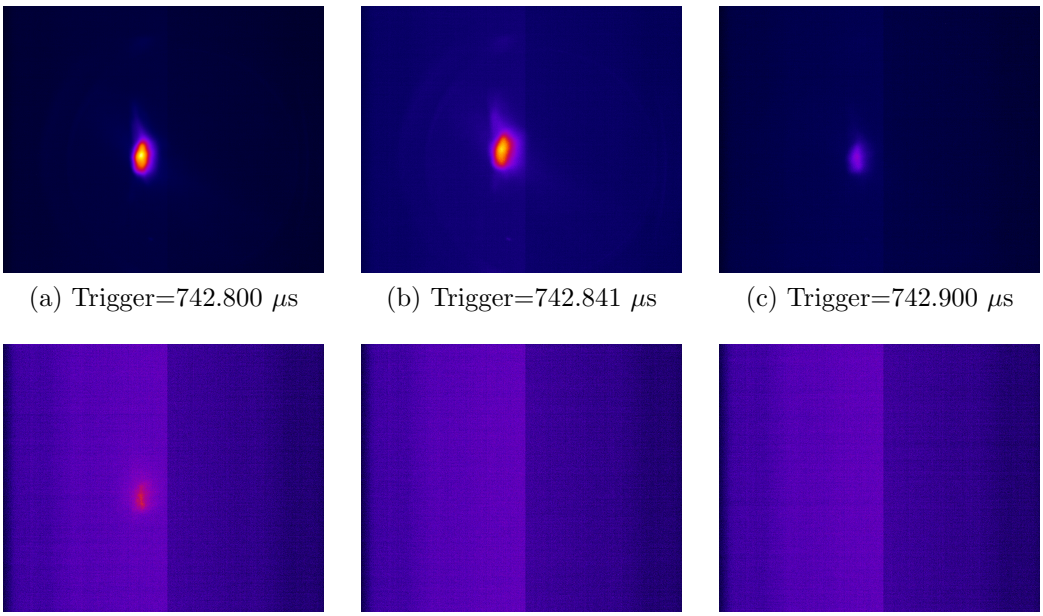

(a) Trigger=742.800 μs (b) Trigger=742.841 μs (c) Trigger=742.900 μs

(d) Trigger=742.800 μs (e) Trigger=742.841 μs (f) Trigger=742.900 μs

Figure 6: Comparision of LYSO:Ce (top row) and OTR (bottom row) intensity versus camera trigger timing.

with an induced current distribution in the metal surface that is larger than the actual transverse beam size.

2.4 Conclusions

Based upon tests conducted at the A0PI, we concluded the transverse profile monitor is ready for mass production. We have verified that our optics system with the GD155000 5 MegaPixel camera can obtain 12-bit images at a 5 Hz rate while meeting the resolution requirement of $<$20 μm with an 18 mm vertica field of view. Also, the YAG:Ce and LYSO:Ce crystals both offer similar performance characteristics for low charge beam, but LYSO:Ce has the added benefit of mitigating the COTR due to the microbunching instability in beam images. The OTR screen can be used to avoid the scintillator saturation at high areal charge density and offer much less beam scattering from thin foils.

3 Image Processing

Basic camera images will be provided to the operator at a rate of either 1 Hz or 5 Hz. Operators will have control over basic camera parameters like shutter width and gain. The software should also inhibit beam for a background image to be taken for dark current subtraction. Also useful will be region of interest marks that note the best location of beam for transmission to the streak camera, interferometers and the center of the beamline. Included on beam display will be x and y projections with Gaussian fits. Important image parameters such as FWHM, sigma, amplitude and centroid should be stored as ACNET parameters. A possible layout of the display screen is shown in Figure 7.

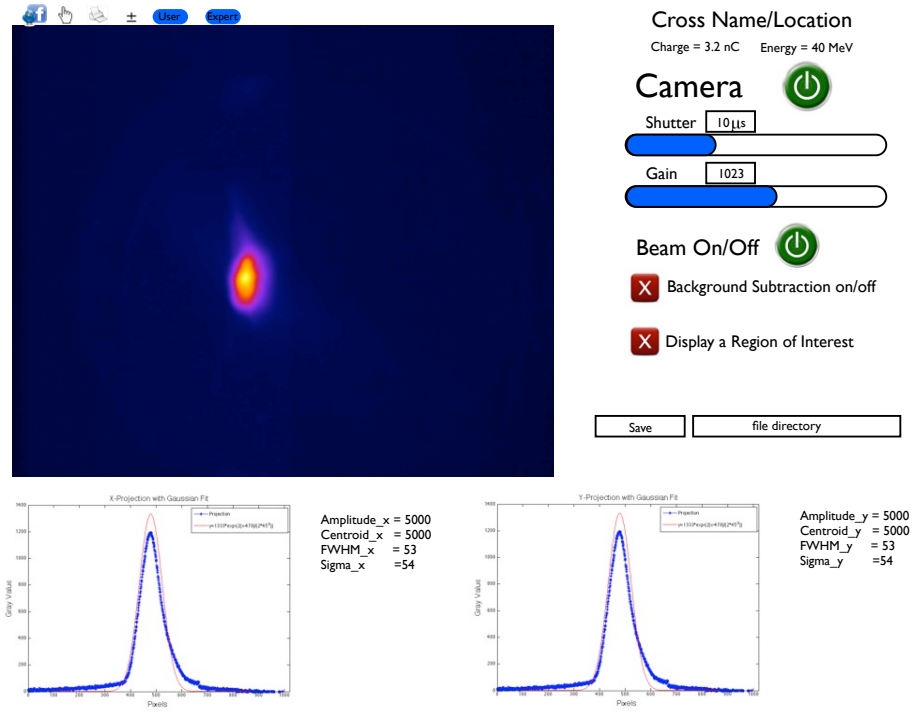

Figure 7: Possible image display for use at ASTA/NML.

A more advanced image processing panel can be selected by the User to allow for the fitting of multiple images. This panel should be based upon the Image Tool software developed by Randy Thurman-Keup and used at the A0PI. While the images do not update in real-time, the User can either

select any number of images to fit or re-process previously saved images. This software also provides complete Gaussian fit information and the ability to average over the summed image or average the individual fits. An example of Image Tool results is shown in Figure 8.

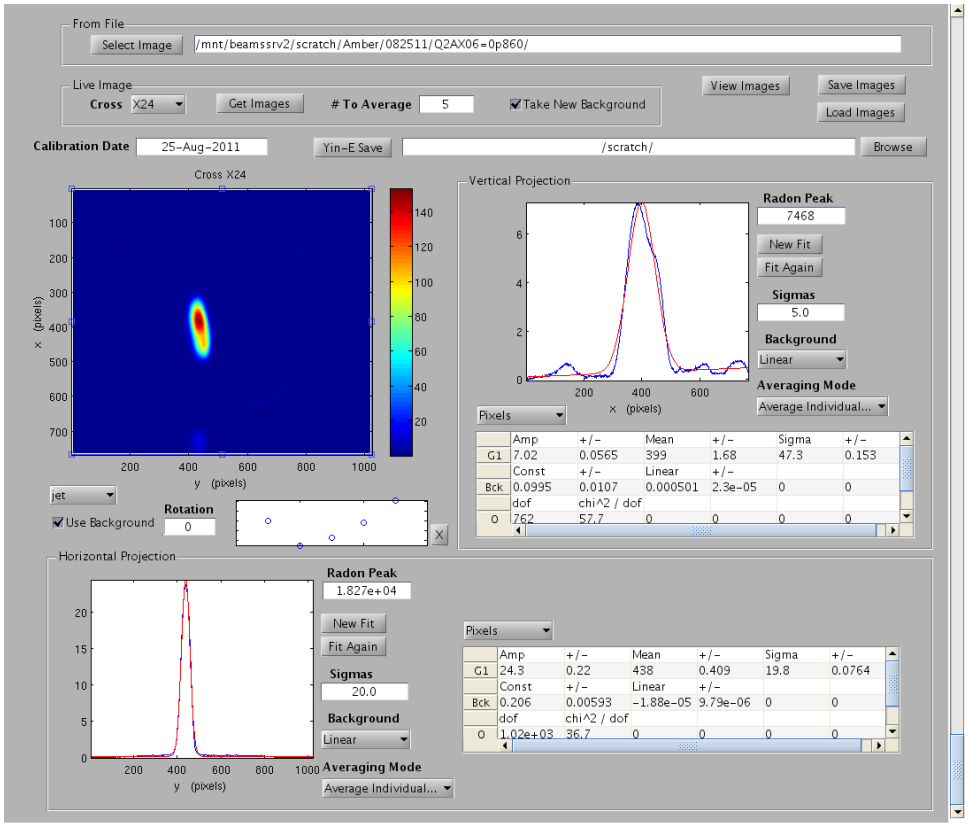

Figure 8: An average of 5 images taken using Image Tool at the A0PI.

As slits will be in use for emittance measurements, an emittance calculator such as the "Transverse Emittance and Phase Space Program" developed for use at the A0PI should be used [13]. The emittance is calculated using the product of the transverse beam size and weighted slit divergence. Phase space reconstruction is also provided.

4 Installation

The station locations and specifications are fully defined in Figure 9 and in the Appendix A. Custom parameters such as the horizontal arm length (L1), vertical tube length (L2), optical assembly orientation either beam left (BL) or beam right (BR) and actuator position up or down are defined in Appendix A. In the prototype the target holder originally made use of only three positions but now the calibration target will be moved from its virtual location to the fourth actuator position. Each position will have a clear aperture of 18 mm.

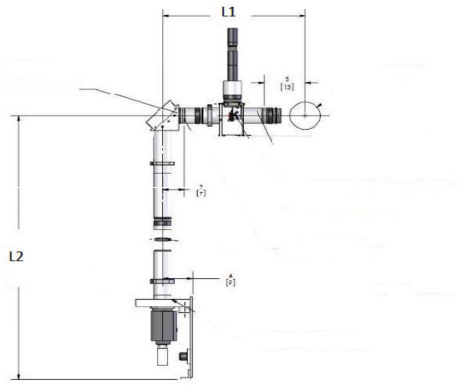

Figure 9: Cross diagram showing L1 and L2 dimensions.

For the pneumatic actuator assembly, the solenoids and limit switches should be connected and wired. Figure 10 shows the solenoid and limit switch connector pinout diagram. Figure 11 shows the solenoid and connector bracket installed. The finger pinch shield needs to be broken into 3 sections.

The optical assembly will be built on a rigid backbone. The prototype design originally called for one filter wheel, but we have chosen to add a second. Table 4 gives the list of what will be installed in both wheels. At the end of the optical assembly will be a 5 Mega pixel camera with a fixed 50 mm lens, see Figure 12 [4].

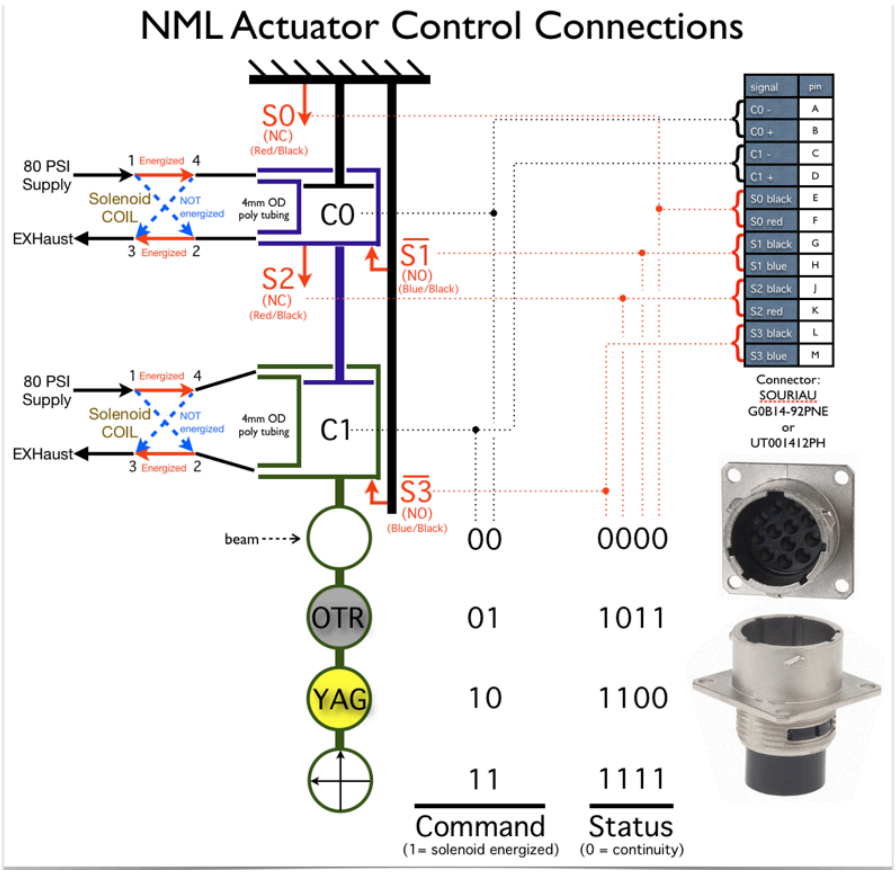

Figure 10: Actuator controls.

4.1 Preparation for Installation

Based upon the installation and testing at the A0PI, the following is an indication of what will be needed for NML [14]:

- Vacuum Cross
  - Target mounting.
  - Technical cleaning at A0.
  - Bake out (∼2 weeks).
  - Vacuum pumping and RGA scans.

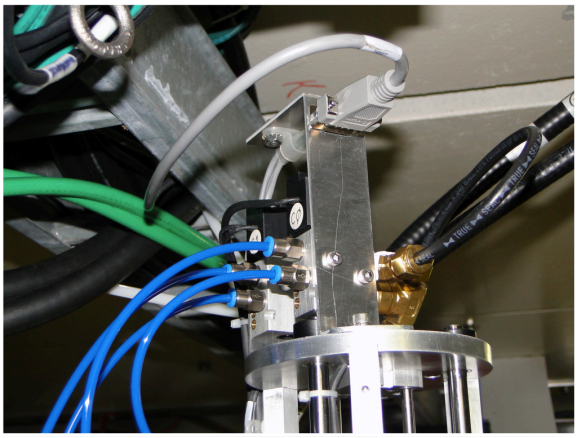

Figure 11: Connector bracket for solenoid.

Table 4: Description of filters in wheels.

Attenuation Wheel	Filter Wheel
1	Clear
0.5	Band Pass 400 ± 20nm
10^{-1}	Band Pass 540 ± 20nm
10^{-2}	Horizontally Polarizing
10^{-3}	Vertically Polarizing

  - Installation into beamline.

- Pneumatic Acutator
  - Solenoid mounting (model Humphrey 410-21-70 12VDC).
  - Limit switch wiring and setting.
  - Pinch shield modifications.
  - Lubrication and functional adjustment.
- Optical System Assembly

Figure 12: Gevicam model GD155000.

  - Filter Wheel.
    - Control system interface.
  - Camera.
    - Server setup and integration.
    - Labview.
    - Fixed 50mm lens, fujinon HFS50A.

- Cabeling.
  - Air lines for solenoids.
  - 24V control for solenoids, see Jim Biggs.
  - Power for camera.
  - Trigger for camera (5Hz).
  - Multi-conductor for filter wheels.
- Controls system interface.

Appendices

A Cross Locations

Location	L1 (mm)	L2 (mm)	Orientation	Total Length (mm)	Actuator Orientation	Scintillator_Target	Scintillator Mirror	OTR Target	OTR_Mirror
108	300	1070	BL	1370	up	YAG:Ce 100 µm	Si:Al 250 µm	Al 25 µm	Si:Al 250 µm
109	300	1070	BL	1370	up	YAG:Ce 100 µm	Si:Al 250 µm	Al 25 µm	Si:Al 250 µm
110	300	1070	BL	1370	up	YAG:Ce 100 µm	Si:Al 250 µm	Al 25 µm	Si:Al 250 µm
115	230	1140	BL	1370	up	YAG:Ce 100 µm	Si:Al 250 µm	Al 25 µm	Si:Al 250 µm
120	300	1070	BL	1370	up	LSO:Ce 100 µm	Si:Al 250 µm	Al 1 µm	Al 1 µm
121	300	1070	BL	1370	up	LSO:Ce 100 µm	Si:Al 250 µm	Al 1 µm	Al 1 µm
124	560	810	BR	1370	down	LSO:Ce 100 µm	Si:Al 250 µm	Al 1 µm	Al 1 µm
126	300	1070	BL	1370	up	LSO:Ce 100 µm	Si:Al 250 µm	Al 1 µm	Al 1 µm
129	300	1070	BL	1370	up	LSO:Ce 100 µm	Si:Al 250 µm	Al 1 µm	Al 1 µm
501	300	1070	BL	1370	up	LSO:Ce 100 µm	Si:Al 250 µm	Al 1 µm	Al 1 µm
502	300	1070	BL	1370	up	LSO:Ce 100 µm	Si:Al 250 µm	Al 1 µm	Al 1 µm
505	300	1070	BL	1370	up	LSO:Ce 100 µm	Si:Al 250 µm	Al 1 µm	Al 1 µm
508	300	1070	BL	1370	up	LSO:Ce 100 µm	Si:Al 250 µm	Al 1 µm	Al 1 µm
511	300	1070	BL	1370	up	LSO:Ce 100 µm	Si:Al 250 µm	Al 1 µm	Al 1 µm
516	300	1070	BL	1370	up	LSO:Ce 100 µm	Si:Al 250 µm	Al 1 µm	Al 1 µm
517	300	1070	BL	1370	up	LSO:Ce 100 µm	Si:Al 250 µm	Al 1 µm	Al 1 µm
518	300	1070	BL	1370	up	LSO:Ce 100 µm	Si:Al 250 µm	Al 1 µm	Al 1 µm
601	300	1070	BR	1370	up	LSO:Ce 100 µm	Si:Al 250 µm	Al 1 µm	Al 1 µm
605	300	1070	BL	1370	up	LSO:Ce 100 µm	Si:Al 250 µm	Al 1 µm	Al 1 µm
608	300	1070	BR	1370	up	LSO:Ce 100 µm	Si:Al 250 µm	Al 1 µm	Al 1 µm
611	300	1070	BL	1370	up	LSO:Ce 100 µm	Si:Al 250 µm	Al 1 µm	Al 1 µm
612	300	1070	BL	1370	up	LSO:Ce 100 µm	Si:Al 250 µm	Al 1 µm	Al 1 µm
701	300	1070	BR	1370	up	LSO:Ce 100 µm	Si:Al 250 µm	Al 1 µm	Al 1 µm
Complete Spare	300	1070	BL	1370	up	LSO:Ce 100 µm	Si:Al 250 µm	Al 1 µm	Al 1 µm
Complete Spare	300	1070	BR	1370	up	LSO:Ce 100 µm	Si:Al 250 µm	Al 1 µm	Al 1 µm
Spare Loaded Cross	NA	NA	BL	NA	up	YAG:Ce 100 µm	Si:Al 250 µm	Al 25 µm	Si:Al 250 µm
Spare Loaded Cross	NA	NA	BL	NA	up	LSO:Ce 100 µm	Si:Al 250 µm	Al 1 µm	Al 1 µm
Spare Loaded Cross	NA	NA	BL	NA	up	LSO:Ce 100 µm	Si:Al 250 µm	Al 1 µm	Al 1 µm
Spare Loaded Cross	NA	NA	BR	NA	up	LSO:Ce 100 µm	Si:Al 250 µm	Al 1 µm	Al 1 µm
Spare Loaded Cross	NA	NA	BR	NA	down	LSO:Ce 100 µm	Si:Al 250 µm	Al 1 µm	Al 1 µm

References

[1] J. Leibfritz, *et al., Proceedings of the 2011 Particle Accelerator Conference* (PAC11), New York, NY, MOP009, (2011).

[2] A. H. Lumpkin, *et al., Proceedings of the 2011 Particle Accelerator Conference* (PAC11), New York, NY, MOP219, (2011).

[3] A. H. Lumpkin *et al.*, Phys. Rev. ST Accel. Beams **14**, 060704 (2011).

[4] `http://www.gevicam.com/images/GD-155000_DS_rev_1_0_10-20-08.pdf`.

[5] `http://www-ssrl.slac.stanford.edu/visa/documents/yagweb-apr-2000.pdf`.

[6] W. Chewpraditku, *et al.* IEEE Trans. Nucl. Sci., vol. 56, no. 6, pp. 38003805, Dec. 2009.

[7] `http://www.apace-science.com/proteus/lyso.htm`.

[8] A. Murokh, "Beam Heating of YAG Crystals", BNL, Oct. 2011.

[9] C. Prokop, *et al.,* Fermilab Technical Memo TM-2516-APC, Sept. 2011.

[10] L. Wartski, *et al.* IEEE Trans. Nucl. Sci., vol. 20, no. 3, pp. 544548, June 1973.

[11] A. H. Lumpkin *et al.*, Phys. Rev. ST Accel. Beams **12**, 080702 (2009).

[12] A. H. Lumpkin, *et al., Proceedings of the 2011 Free Electron Laser Conference* (FEL11), Shanghai, China, THPB19, (2011).

[13] R. Thurman-Keup, *et al., Proceedings of the 2011 Particle Accelerator Conference* (PAC11), New York, NY, MOP226, (2011).

[14] B. Flora, *Preliminary RadiaBeam Testing.*